PNAS RESEARCH ARTICLE | PLANT BIOLOGY OPEN ACCESS

The white lupin CCR1 receptor-like kinase controls systemic Autoregulation of Cluster Root and Nodule Development

Laurence Marquès[a,1], Fanchon Divol[a], Alexandra Boultif[a], Fanny Garcia[a], Alexandre Soriano[a,2], Cléa Maurines-Carboneill[a], Virginia Fernandez[a], Inge Verstraeten[a,3], Hélène Pidon[a,2], Esther Izquierdo[a], Bárbara Hufnagel[a,4], and Benjamin Péret[a,1]

Affiliations are included on p. 11.

Edited by Éva Kondorosi, Hungarian Academy of Sciences, Biological Research Centre, Szeged, Hungary; received September 21, 2024; accepted April 4, 2025

Root development is tightly regulated in plants to optimize nutrient acquisition and interactions with soil microorganisms. In legumes, the Autoregulation of Nodulation (AoN) pathway systemically controls the proliferation of root nodules, which are energy-intensive organs. Mutations affecting the AoN pathway result in a hypernodulation phenotype accompanied by altered root development. However, it remains unclear whether this modification of root development is also systemic and coordinated with nodulation. In this study, we report the identification of the *constitutive cluster root 1 (ccr1)* mutant in white lupin (*Lupinus albus*), which exhibits constitutive production of an excessive number of cluster roots. We demonstrate that CCR1 is an ortholog of *HAR1/SUNN/NARK* leucin-rich repeat-receptor like kinases (LRR-RLKs), which are key regulators of the AoN pathway. Furthermore, we show that *CCR1* negatively regulates both nodule and cluster root development. Interspecific grafting experiments between white and narrow-leaved lupin (*Lupinus angustifolius*), a species incapable of producing cluster roots, show that *ccr1* shoots can induce the formation of cluster-like roots in narrow-leaved lupin rootstocks. This highlights the conservation of a CCR1-dependent signaling cascade. Transcriptome analyses reveal that *CCR1* targets the conserved NIN/LBD16-NFYA regulatory module, which connects nodule and lateral root development through a shared inhibitory systemic pathway. We propose that this pathway represents a broader developmental control mechanism of root organogenesis, termed Autoregulation of Cluster Root and Nodule Development (AoDev).

root development | cluster root | autoregulation | LRR-RLK | Lupinus

Significance

Plants adapt root and shoot development to environmental cues through systemic signaling pathways. In white lupin (*Lupinus albus*), we identified mutants with excessive cluster roots that also exhibited hypernodulation. The responsible gene, *LalbCCR1*, encodes a leucine-rich-repeat receptor-like kinase (LRR-RLK), an orthologue of the HAR1/SUNN/NARK receptors central to Autoregulation of Nodulation (AoN). This gene regulates nodule formation and cluster root development via the NIN/LBD16-NFYA module. This mechanism, termed Autoregulation of Cluster Root and Nodule Development (AoDev), highlights the pivotal role of a single LRR-RLK in orchestrating nodulation and cluster root formation, providing a unified framework linking systemic signaling to coordinated root organogenesis.

Plasticity of plant root development drives the exploitation of soil resources to meet the demand for nutrients. Systemic integration pathways play a central role in coordinating plant growth. Specifically, the demand for nitrogen (N) triggers a cascade of signaling events that orchestrate systemic responses to optimize nutrient uptake and allocation (1, 2). Recent studies have highlighted the involvement of root-secreted small peptides and their cognate leucine-rich repeat receptor-like kinases (LRR-RLK) as pivotal regulators of local cell-to-cell communication and systemic root-to-shoot-to-root signaling pathways (3, 4). These pathways are of critical importance in both governing plant-wide developmental processes and maintaining nutrient homeostasis, ultimately contributing to optimal plant fitness.

In legume plants, Autoregulation of Nodulation (AoN) has long been recognized as a pivotal negative systemic regulator of nodulation induced by rhizobial colonization (5–7). Its characterization has been achieved through a combination of EMS-based forward genetics, natural variation approaches, and grafting experiments in model species such as *Lotus japonicus*, *Glycine max,* and *Medicago truncatula* (8–11). Under conditions of nitrate deficiency, legume roots are predisposed to colonization by N-fixing rhizobacteria, resulting in the formation of symbiotic nodules. The AoN pathway encompasses two distinct mechanisms that finely tune the regulation of root nodulation to balance shoot and root development, thereby preventing excessive proliferation of energy-consuming nodules (7, 12). The first mechanism involves the production of CLAVATA3/EMBRYO SURROUNDING REGION-RELATED (CLE) peptides in the roots, followed by their translocation via the xylem to the shoot. Upon reaching the shoot, CLE peptides interact with LjHAR1/GmNARK/MtSUNN LRR-RLK receptors, triggering the inhibition of nodulation via a rootward inhibitory signal. The second mechanism, elucidated in *M. truncatula,* and also responsive to nitrate supply, involves the action of root-secreted C-TERMINALLY ENCODED PEPTIDE (CEP) peptides and the MtCRA2 LRR-RLK receptor in shoot tissues. This mechanism not only governs lateral root development but

[1]To whom correspondence may be addressed. Email: laurence.marques@umontpellier.fr or benjamin.peret@cnrs.fr.

[2]Present address: Unité Mixte de Recherche Amélioration Génétique et Adaptation des Plantes Méditerranéennes et Tropicales Institut, Centre de Coopération Internationale en Recherche Agronomique Pour le Développement, Montpellier 34000, France.

[3]Present address: HortiRoot, Department Plants and Crops, Faculty of Bioscience Engineering, Ghent University, Ghent B-9000, Belgium.

[4]Present address: Unité Mixte de Recherche Amélioration Génétique et Adaptation des Plantes Méditerranéennes et Tropicales Institut, Centre de Coopération Internationale en Recherche Agronomique Pour le Développement, Petit-Bourg, Guadeloupe F-97170, France.

This article contains supporting information online at https://www.pnas.org/lookup/suppl/doi:10.1073/pnas.2418411122/-/DCSupplemental.

Published May 22, 2025.

also, unlike the CLE-dependent route, activates nodulation (13). The microRNA miR2111c and TOO MUCH LOVE (TML) Kelch-repeat F-box proteins have been identified, in both routes, as components of the downward signaling cascade (14–16).

White lupin (WL, *Lupinus albus*) is a legume crop capable of thriving in N- and phosphate (P)-deficient soils, owing to the remarkable developmental plasticity of its root system (17, 18). In response to N deficiency, WL roots form N-fixing nodules through symbiotic interaction with bacteria from *Bradyrhizobium* genus. Additionally, P starvation triggers the development of specialized lateral roots (LRs) known as cluster roots (CRs) (19). They are characterized by densely clustered, short third-order lateral roots termed rootlets, which are highly nutrient-efficient organs (20, 21). In contrast, the closely related species narrow-leaved lupin (NLL, *Lupinus angustifolius*) does not produce CRs (22). Despite the fact that WL has been employed as a model for CR exsudative activities, it remains unclear how they are induced and how their development is controlled at the whole plant level.

Here, we conducted a genetic screen of a mutagenized WL population to identify mutants that constitutively produce CRs under P-rich, typically suppressive, conditions. This screening led to the identification of the *LalbCCR1* gene (*CONSTITUTIVE CLUSTER ROOT 1*), which encodes a Leucine Rich Repeat-Receptor Like Kinase (LRR-RLK). *LalbCCR1* shares synteny with three LRR-RLK genes, *LjHAR1, GmNARK,* and *MtSUNN,* which control AoN in *Lotus*, *Glycine max* (soybean), and *Medicago*, respectively. Our findings demonstrate that *LalbCCR1* functions within a systemic pathway, reminiscent of AoN, limiting both CR and nodule initiation via the NIN/LBD16-NFYA module. The involvement of *LalbCCR1* in this root developmental pathway suggests a role in reducing the formation of carbon-intensive organs, even in the absence of rhizobial symbiosis and under N-rich conditions. We propose the term Autoregulation of Cluster Root and Nodule Development (AoDev) for this systemic inhibitory regulatory mechanism of root organogenesis.

Results

Genetic Identification of *LalbCCR1* as an LRR-RLK Inhibiting CR Development. In phosphate-deficient medium (-P), white lupin produces numerous CRs in the upper part of the root system, whereas P-rich medium (+P) inhibits their development (Fig. 1*A*). We screened 800 M2 batches of an ethyl-methanesulfonate (EMS)-mutagenized WL AMIGA population for plants exhibiting numerous CRs in the P-rich suppressive condition. We identified four independent lines of recessive mutants (ems5, ems96, ems120, and ems413). These mutants consistently develop two to five times more CRs compared to wild-type plants independently of the P supply (Fig. 1 *A* and *B* and *SI Appendix*, Fig. S1*A*). They also have shorter lateral and primary roots resulting in a marginally reduced dry weight compared to wild-type (Fig. 1*B* and *SI Appendix*, Fig. S1*B*). The total number of LR is increased in the mutants compared to wild-type (*SI Appendix*, Fig. S1*C*). Notably, *ccr1* mutants produce a high number of very short secondary roots with determinate growth, along the primary root. CRs of the mutants display a higher rootlet density, as if all the potential sites of tertiary LR initiation had been unlocked (Fig. 1 *C* and *D*). Physiologically, the CRs of the mutants are fully active, excreting large amounts of protons, and displaying elevated phosphatase and reductase activities (*SI Appendix*, Fig. S1*D*).

The mutations are recessive, segregate with the mutant phenotype, and the four independent mutants fall into the same

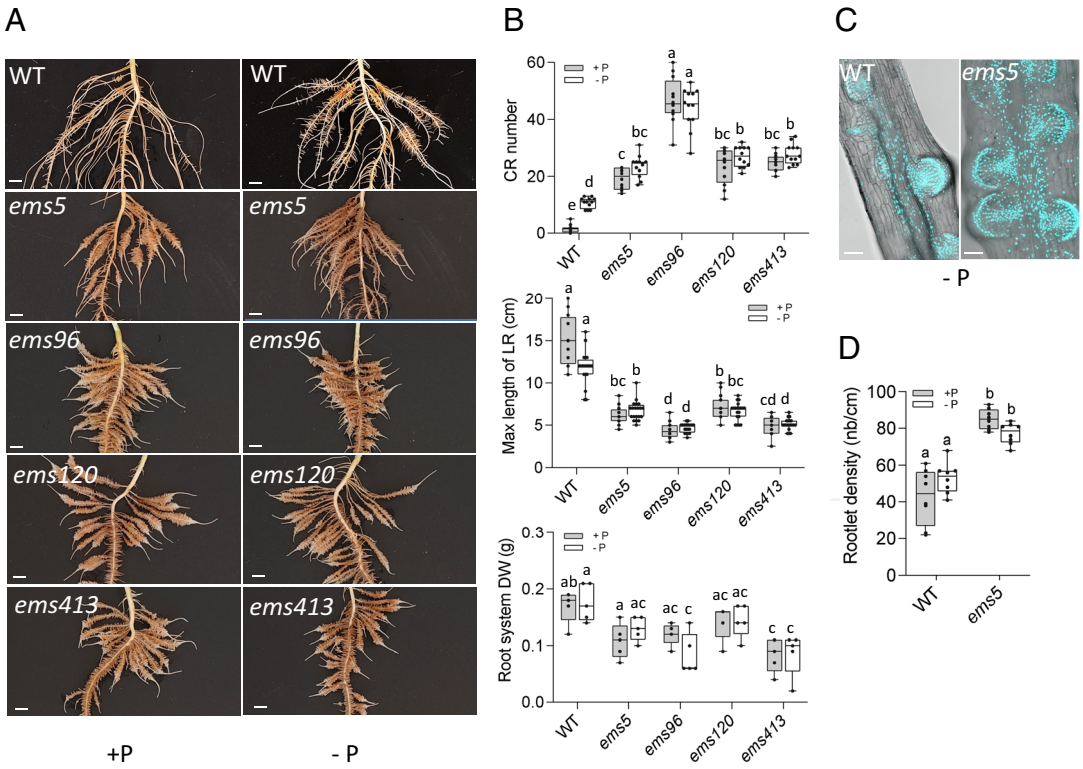

Fig. 1. Phenotypes of the four allelic *ccr1* mutants. (*A*) Representative images of the upper part of the root system from 20-d-old wild-type (WT) and the four *ccr1* mutant plants grown on either phosphate-rich medium (+P) or phosphate-deficient medium (−P). (Scale bar, 1 cm.) (*B*) Quantitative analysis of various root traits in wild-type (WT) and *ccr1* mutant plants, including CR abundance within the upper 10 cm of the root systems, maximum lateral root length, and root system dry weight. Statistical analysis was performed using two-way ANOVA with Tuckey correction, $P < 0.05$. (*C*) Apotome imaging of a CR section from the *ems5* mutant compared to wild-type (WT) plants. DAPI staining revealed rootlet primordia, identifiable by their small nuclei. (Scale bar, 100 µm.) (*D*) Density distribution of rootlets along 1 cm of cluster root in the *ems5* mutant. Statistical analysis was performed using two-way ANOVA with Tuckey correction, n = 8, $P < 0.05$.

complementation class that we named *ccr1* (*constitutive cluster root 1*) (*SI Appendix*, Fig. S2 *A* and *B*). Bulk-Segregant Analysis combined with mapping-by-sequencing (BSA-seq) was performed in parallel on the four allelic *ccr1* mutant lines. This analysis unveiled a linkage of causal mutations to the beginning of chromosome 3 in all four *ccr1* lines (*SI Appendix*, Fig. S2*C*). Further analysis of this genomic region across the four *ccr1* alleles pinpointed the presence of causal SNPs within the *CONSTITUTIVE CLUSTER ROOT 1* gene (*LalbCCR1, Lalb_Chr03g0025491,* https://www.whitelupin.fr). *LalbCCR1* encodes a putative protein-like kinase of the LRR-RLK family XI-1 (Fig. 2*A*) with a canonical 3D-structure calculated by homology modeling using ColabFold v1.5.5: AlphaFold2 with MMseqs2 (Fig. 2*B*). Specifically, the *ccr1-2* allele carries a G1370A SNP resulting in a premature stop-codon within the LRR domain; both *ccr1-1* and *ccr1-3* alleles contain a G2099A SNP causing a G700E substitution in the kinase domain; and *ccr1-4* exhibits a C2437T SNP resulting in an H813Y change within the kinase domain (Fig. 2*A*). The G > E substitution found in *ccr1-1* and *ccr1-3* is also present in a *LalbCCR1* paralog, that we named *LalbCCR1-like* (*LalbChr01g0002311*; Fig. 2*C*). The pangenome analysis of WL confirms the presence of this SNP in *LalbCCR1-like* across all WL accessions (23). In order to describe

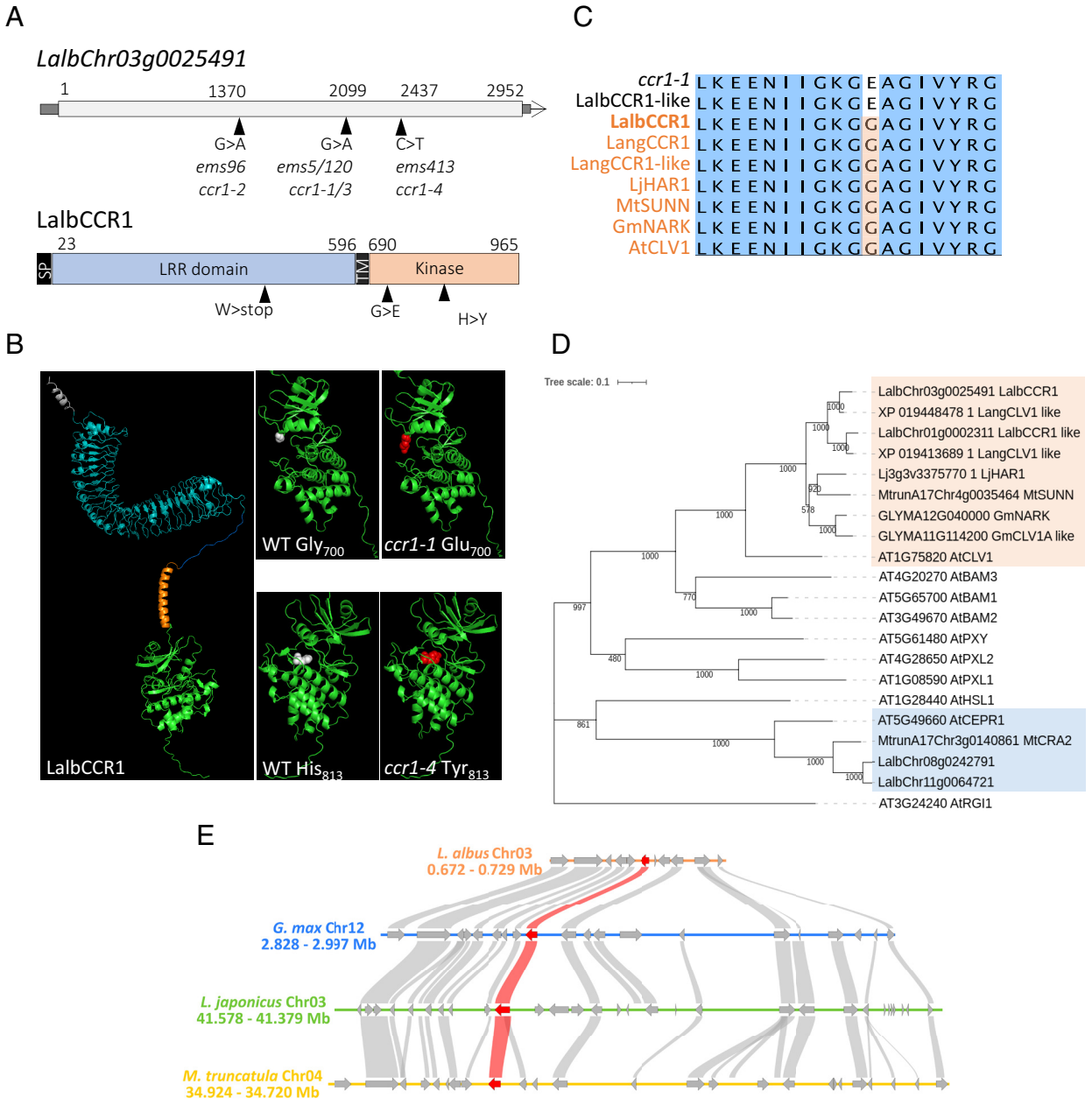

Fig. 2. LalbCCR1 is an LRR-RLK syntenic with LRR-RLKs involved in Autoregulation of Nodulation (AoN). (*A*) *LalbCCR1* gene (*LalbChr03g0025491*) and LalbCCR1 protein structures. The *LalbCCR1* gene lacks introns. EMS-induced mutations are indicated by a triangle with the corresponding mutant names. The predicted LalbCCR1 protein contains an LRR domain, a transmembrane domain, and a kinase domain. The specific amino acid substitutions resulting from EMS-induced SNPs are given. (*B*) The 3D-structural model of LalbCCR1 generated by AlphaFold2, highlighting the mutated amino acid positions within the kinase domain of *ccr1-1* and *ccr1-4* mutants. (*C*) Allelic variations in the kinase domain segment containing the *ccr1-1/3* G > E mutation across closest-homologs of LalbCCR1 in *Lupinus albus*, *Lupinus angustifolius, Lotus japonicus*, *Glycine max*, *Medicago truncatula,* and *Arabidopsis thaliana.* Notably, the *LalbCCR1* paralog, *LalbCCR1-like* exhibits the same punctual mutation observed in *ccr1-1/3* mutants, leading to a nonfunctional protein in *L. albus*. (*D*) Phylogenetic tree of LalbCCR1-related proteins across Narrow-Leaved Lupin (NLL, *L. angustifolius*), *Lotus japonicus*, *Glycine max*, *M. truncatula* and *Arabidopsis thaliana*. Proteins with homologous relationships to AtCLV1 are highlighted with orange background, while those homologous to MtCRA2 are highlighted with blue background. (*E*) Syntenic relationships among *LalbCCR1, GlmNARK, LjHAR1,* and *MtSUNN* loci, indicating genomic organization across species at this locus.

the relationship between *LalbCCR1*, *LalbCCR1-like,* and other ortholog genes, a phylogenetic tree was constructed, including ten of the nearest BLAST-sequence homologs of *LalbCCR1* in *Arabidopsis thaliana*, and LRR-RLKs from model legumes known to be involved in AoN: *LjHAR1*, *GmNARK, MtSUNN*, and *MtCRA2* (Fig. 2*D*). *LalbCCR1* clustered with *GmNARK*, *LjHAR1*, *MtSUNN*, as the nearest *LRR-RLK/XI* homolog of *AtCVL1.* Further analysis of genomic loci revealed that the three legume *LRR-RLK* genes *MtSUNN, LjHAR1, GmNARK* are syntenic to *LalbCCR1* (Fig. 2*E*).

LalbCCR1 Controls CR and Nodule Development through a Systemic Shoot-to-Root Signaling Pathway. *MtSUNN, LjHAR1,* and *GmNARK* are well known to be involved in AoN with corresponding mutants displaying remarkable supernodulation phenotypes (5, 11, 24, 25). Based on the synteny observed between *LalbCCR1* and these three LRR-RLKs, we assessed the nodulation phenotype of the independent *ccr1-1* and *ccr1-2* mutants after inoculation with *Bradyrhizobium lupini.* Both mutant lines exhibited hypernodulating phenotypes (*SI Appendix*, Fig. S3 *A–F*). The efficiency of nitrogen fixation was highlighted by the healthier appearance and greener foliage of nodulated plants compared to the non-nodulated ones, as well as by the reddish coloration of the nodules. The hypernodulation phenotypes of the *ccr1* mutants provide additional validation for the accurate identification of the causal gene. We then used grafting experiments to test the systemic nature of hypernodulation phenotypes observed in *ccr1* mutants. Our results demonstrated that *ccr1* shoots promote hypernodulation, characterized by clusters of nodules intertwined with short rootlets, when grafted onto wild-type roots (Fig. 3 *A–C* and *SI Appendix*, Fig. S3 *G–J*). Analysis of *LalbCCR1* expression in various WL organs revealed predominant expression in petioles and hypocotyls (*SI Appendix*, Fig. S4), in agreement with its function as a shoot regulator.

Subsequently, we conducted grafting experiments to test whether CCR1 inhibition of cluster roots is also systemic. All grafting experiments were conducted under P-rich conditions, which are favorable for the grafting process and known to inhibit CR development. In this CR-suppressing condition, significant CR development occurred when *ccr1* shoots were grafted onto wild-type rootstocks, while conversely, grafting wild-type shoots significantly inhibited CR formation on *ccr1* rootstocks (Fig. 3 *D* and *E* and, for *ccr1-2, SI Appendix*, Fig. S5 *A* and *B*).

***LalbCCR1*-Mediated Control of LR Development Extends Beyond White Lupin Species.** We next tested whether the CCR1-dependent inhibitory signal is specific of WL. Since NLL is unable to produce CRs, we performed interspecific grafting

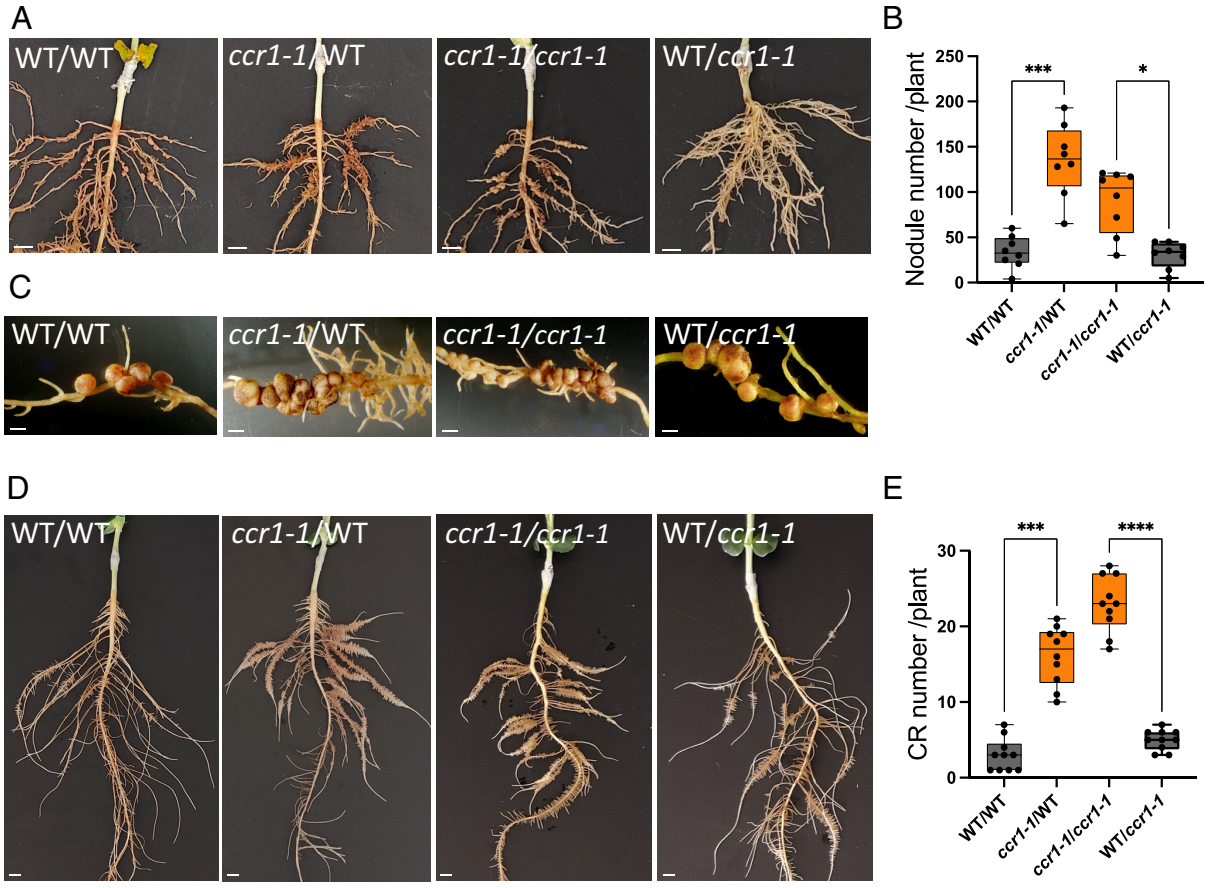

Fig. 3. *LalbCCR1* controls CR nodulation via a systemic signaling pathway. (*A*) Representative images of nodulated rootstocks of the four 3-week-old graft combinations between wild-type (WT) and *ccr1-1* mutant. The plants were inoculated with *Bradyrhizobium lupini*. The legends of the images indicate scion/rootstock. (Scale bar, 0.7 cm.) (*B*) Quantification of nodule numbers per plant on the rootstocks of the four 3-week-old graft combinations between wild-type (WT) and *ccr1-1* mutant. The legends of the images indicate scion/rootstock. Error bars represent mean ± SD, with statistical analysis performed using the Kruskal–Wallis test, n = 8, **P*-value = 0.0305, ****P*-value = 0.0003. (*C*) Magnification of the nodules formed on the rootstocks of grafted plants, revealing compact clusters of nodules on *ccr1-1*/WT and *ccr1-1*/ *ccr1-1* plants. The legends of the images indicate scion/rootstock. (Scale bar, 0.2 cm.) (*D*) Root systems of the four 3-week-old graft combinations between wild-type (WT) and *ccr1-1* mutant. The legends of the images indicate scion/rootstock. Heterografted plants, *ccr1-1*/WT and WT/*ccr1-1*, demonstrate that the constitutive CR phenotype is primarily influenced by the *ccr1-1* mutation in the scion rather than in the rootstock. (Scale bar, 1 cm.) (*E*) Quantitative assessment of CR abundance within the upper 10 cm of the rootstocks. Error bars represent mean ± SD, and statistical analysis was performed using the Kruskal–Wallis test, n = 10, ****P*-value = 0.0006, *****P*-value < 0.0001.

experiments between WL and NLL. Grafting *ccr1* mutant shoots onto NLL rootstocks induced a remarkable transformation in NLL root architecture, leading to the development of clusters of short tertiary roots that could be described as CR-like (Fig. 4 *A* and *B*). The phenotypes are even more striking with the null allele *ccr1-2* (*SI Appendix*, Fig. S5*C*). This significant modification of root architecture occurred in P-rich medium, suggesting that the P-starvation signal is not involved in this response. We also observed that grafting wild-type WL shoots onto NLL rootstocks, triggered the development of some tertiary short roots, albeit to a lesser extent than when *Lalbccr1* was used as scion. A dose–effect relationship was observed in the induction of CR development of NLL rootstocks across the three grafting scenarios: NLL/NLL, WL/NLL, and *Lalbccr1*/NLL, with an increasing proportion of short tertiary roots respectively (Fig. 4 *A* and *B*). An inverse developmental gradient was observed when *Lalbccr1* was used as rootstock. Grafting wild-type WL shoots onto *Lalbccr1* rootstocks inhibited CR development, albeit to a lesser extent than when NLL was used as scion (Fig. 4 *C* and *D*, for *ccr1-2* and *SI Appendix*, Fig. S5 *B* and *D*). Indeed, NLL shoots profoundly and strikingly inhibited the development of CRs on *ccr1* roots. Correlatively, neither *LangCCR1* nor *LangCCR1-like* carry the *ccr1-1* SNP suggesting that NLL probably has two functional LRR-RLK CCR1 that inhibit CR formation whereas WL has only one (Fig. 2*D*). These allelic variations in CCR1 and CCR1-like LRR-RLKs between WL and NLL well correlates with the observed phenotypic gradient in the grafting experiments.

Lateral Root Developmental Genes are Involved in early CR Development. White lupin CRs undergo successive emergence of numerous rootlets along one LR, establishing a continuous spatial and temporal gradient of developmental stages. Taking advantage

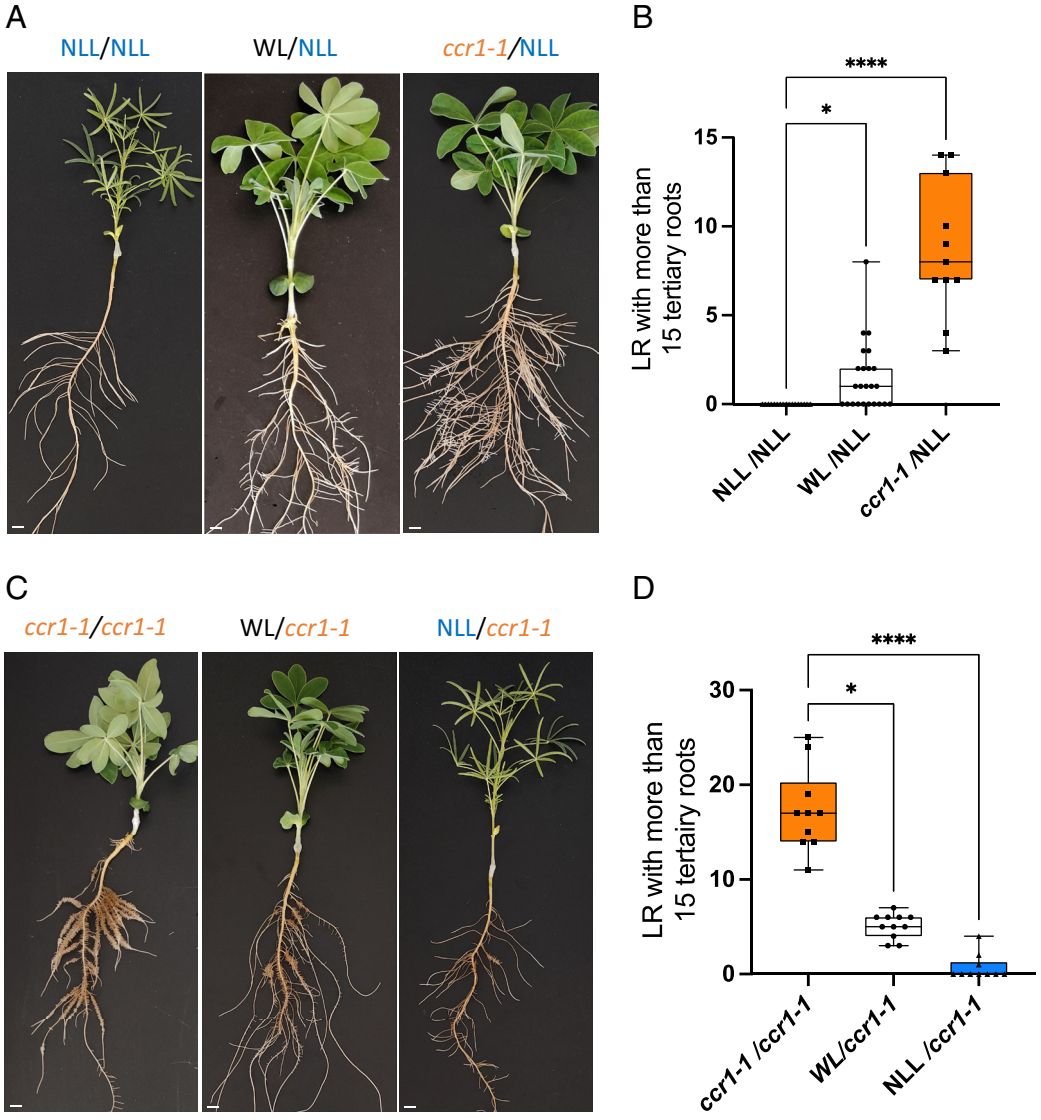

Fig. 4. Phenotypes of interspecific grafts between *L. albus*, *L. angustifolius*, and the *ccr1-1* mutant. (*A*) Representative images illustrating rootstocks phenotypes of grafted plants using NLL (*L. angustifolius*) as rootstock and NLL, WL (*L. albus)* or the mutant *ccr1-1* as scions. The *ccr1-1* scion allowed the emergence of numerous tertiary roots on NLL rootstock. Legends of the images indicate the scion/rootstock combination. (Scale bar, 1 cm.) (*B*) Quantitative evaluation of the abundance of LR with more than 15 tertiary rootlets on NLL rootstocks, with statistical analysis performed using the Kruskal–Wallis test; n = 11 to 24; adjusted *P*-values are indicated: *$P = 0.0110$, ****$P < 0.0001$. (*C*) Representative images illustrating rootstocks phenotypes of grafted plants using the *ccr1-1* mutant as rootstock and NLL *(L. angustifolius),* WL (*L. albus), or ccr1-1* as scions. The NLL scion markedly suppressed the formation of CRs on *Lalbccr1-1* rootstock, whereas WL did so to a lesser extent. Notably, *LalbCCR1-like* gene carried the same mutation as in the *ccr1-1* mutant, whereas *LangCCR1-like* does not. Legends of the images indicate the scion/rootstock combination. (Scale bar, 1 cm.) (*D*) Quantitative evaluation of the abundance of LR with more than 15 tertiary rootlets on *ccr1-1* rootstocks, with statistical analysis performed using the Kruskal–Wallis test, n = 10 to 11, adjusted *P*-values are indicated: *$P = 0.013$, ****$P < 0.0001$.

of this model, we conducted sampling of rootlet formation by collecting 1 cm-long root segments every 12 h, up to 132 h as described before (26) to generate a comprehensive temporal transcriptomic dataset of cluster root development. Additionally, pieces of LRs were utilized as control (Fig. 5*A* and Dataset S1). Principal component analysis of sample distribution delineates an elliptical trajectory progressing from state T000, proximal to LR, to timepoints T024-036-048 (hours), which exhibit the greatest deviation from LR samples along axis 1. These three T024-036-048 samples are not distinctly differentiated, unlike the more consistent states observed at T120 and T132, when rootlets had completed their growth (Fig. 5*B*). In order to identify genes

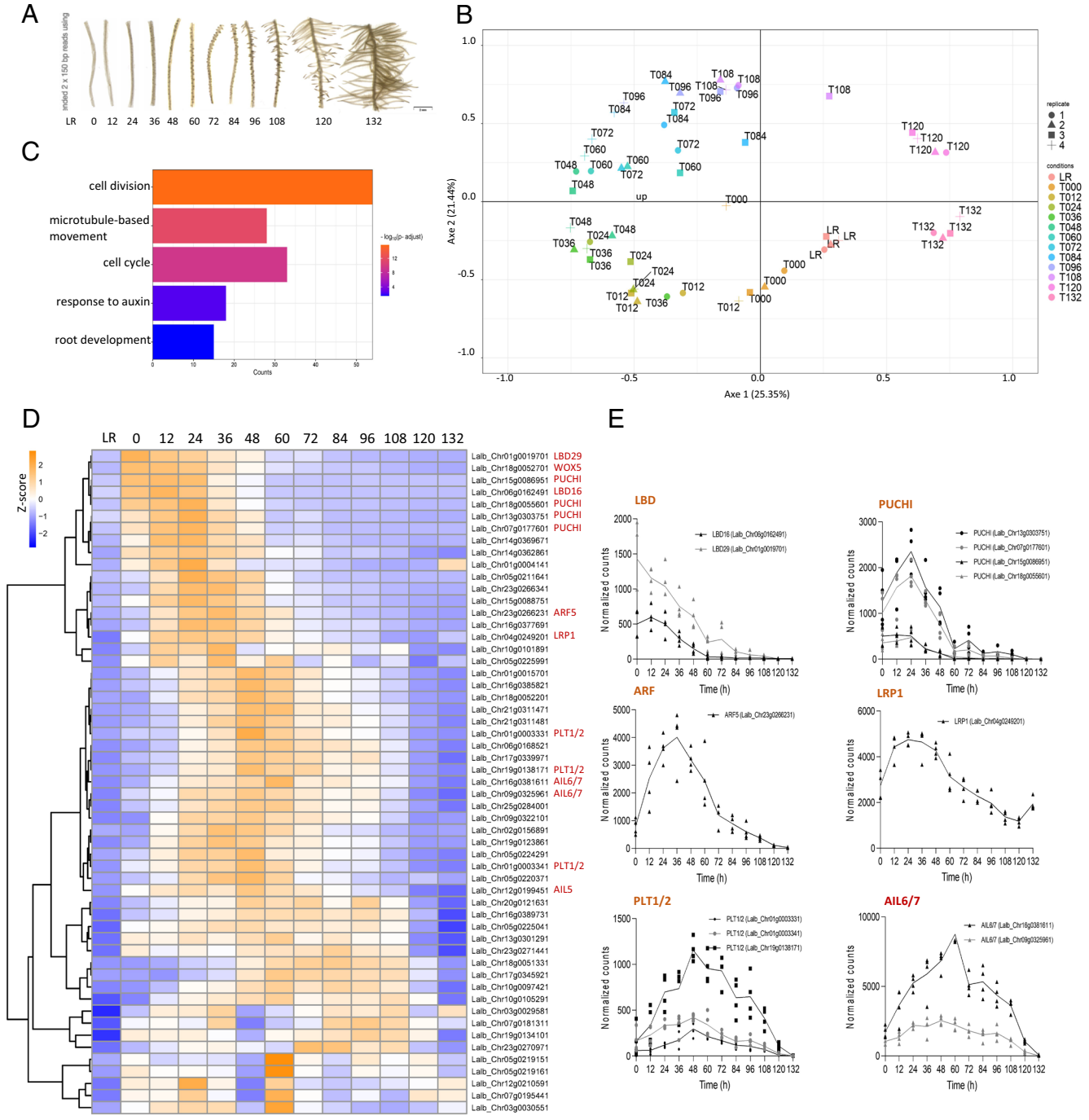

Fig. 5. Transcriptional expression analysis during CR formation in white lupin. (*A*) Illustrations depicting the developmental stages of 1-cm long segments of LR sampled for developmental temporal RNAseq transcriptome analysis. Samples were collected every 12 h over a period of 132 h. Segments of LR without developing rootlets served as control. Four biological replicates were performed, each containing eight 1-cm-long LR segments coming from four different plants. (Scale bar, 2 mm.) (*B*) Scatter plot presenting the distribution of the RNAseq dataset with the four replicates for each timepoint and LR control samples in the two principal components, explaining 46.79% of the total variance. (*C*) GO enrichment analysis of early up-regulated genes between LR and timepoints T024-036-048 [Absolute Log2(fold change) > 2, FDR < 0.05]. GO terms presenting counts > 10 are displayed. They are associated with cell division, response to hormones, and root development. Normalization, differential expression, and GO term analysis were performed using the DIANEbeta R package (28). (*D*) Clustered heatmap displaying the normalized Z-scores of gene expression for up-regulated transcription factors from 8 families known to be involved in root development (AP2/EREB, LOB domain, ARF, GRAS, Homeodomain, NAM, PLATZ, and STY-LRP1), comparing LR with timepoints T024-036-048 [Absolute Log2(fold change) > 2, adjust *P*-value (FDR) < 0.05]. Transcription factors known to participate in *A. thaliana* LR patterning are highlighted. (*E*) Kinetic profiles illustrating changes over the 132 h early developmental stages of six major LR patterning transcription factors involved in CR development.

specifically expressed during the early developmental stages of rootlets, we retrieved 2,349 differentially regulated genes between LR and timepoints T024-036-048 [Absolute Log2(fold change) > 2; FDR < 0.05] (Dataset S2). Subsequent Gene Ontology (GO) enrichment analysis highlighted terms associated with "cell division," "cell cycle," "response to auxin," and "root development," among the up-regulated genes with the most prevalent counts likely identifying early developmental stages of rootlet formation (Fig. 5*C* and Dataset S3). Conversely, GO enrichment analysis of down-regulated genes resulted in a less interpretable outcome, with numerous GO terms spanning diverse pathways (*SI Appendix*, Fig. S6 and Dataset S3). We next decided to focus on up-regulated transcription factors. Filtration shortlisted 144 genes (Dataset S4) and we compiled a list of transcription factor genes up-regulated from 8 families known to be involved in root development: AP2/EREB, LOB domain, ARF, GRAS, Homeodomain, NAM, PLATZ, and STY-LRP1 (Dataset S5). We retrieved 55 WL genes, with the AP2/EREB family representing nearly half with a total of 27 genes. Within the AP2/EREB family, we identified genes associated with ethylene and cytokinin signaling, such as ERF and CRF, alongside well-characterized genes implicated in early LR patterning, including 4 PUCHI, 2 AIL6/7, and 3 PLT1/2 genes. Additionally, within other families, we identified genes crucial for LR development, including LBD16, LBD29, WOX5, LRP1, SMB, and SCR (Fig. 5*D*). The temporal expression patterns of these genes align closely with well-established transcriptional dynamics observed in *A. thaliana* LR development datasets (27), providing compelling evidence that rootlets undergo analogous developmental processes as LR (Fig. 5*E*) and pinpointing sets of early and dynamic gene expression patterns as potential targets of the AoDev pathway.

The NIN/LBD16-NFYA Module Is Upregulated in *ccr1* Plants Independently of Rhizobial Infection. To elucidate the regulatory role of *LalbCCR1* in CR development and identify potential targets of AoDev, we performed an RNAseq transcriptome analysis focusing on LR transitioning into CR, in wild-type *versus ccr1-1* mutant plants (Fig. 6*A* and Dataset S6). Differential gene expression analysis between wild-type and *ccr1-1* [Absolute Log2(fold change) > 1; FDR < 0.05], identified 1,845 differentially expressed genes, including 798 upregulated genes, of which 125 encode transcription factors (Dataset S7). Among these, 28 were also upregulated during the early stages of CR development (Fig. 6*B* and Dataset S8 "Common genes in the Venn diagram"). Notably, transcription factors such as LBD16, LBD29, WOX5, PUCHI, AIL6/7, and PLT1/2 were found. These results were confirmed in another *ccr1* allele by measuring gene expression levels on LRs transitioning into CRs from *ccr1-2* plants by RT-qPCR (*SI Appendix*, Fig. S7*A*). Using two complementary transcriptomic approaches, we revealed that genes expressed early during CR development and known to be important regulators in other models for LR development, such as LBD16, are up-regulated in the *ccr1* mutants.

Analyzing the deregulated genes between *ccr1-1* mutant and wild-type plants, we observed that *CLE* and *TML* genes exhibited the expected regulatory patterns corresponding to their role in AoN: up-regulation for some CLE and down-regulation for TML (Fig. 6*C*). Unexpectedly, we found that two *NIN* genes and two *NF-YA* genes, involved in the late developmental stage of the symbiotic pathway, were slightly but significantly up-regulated in *ccr1-1* plants compared to wild-type, while other genes involved in the early signaling events of the nodulation pathway, including *SYMRK*, *CCamK*, or *NSP1*, did not show significant up-regulation in *ccr1-1* background (Fig. 6*C* and Dataset S8). These results were confirmed for *NIN*, *NF-YA,* and *NSP1* by RT-qPCR expression analysis in another *ccr1* allele (*ccr1-2)* (*SI Appendix*, Fig. S7*B*). We next investigated whether the observed regulation of *NIN* and *NF-YA* in *ccr1* mutant was due to local or systemic events. LRs transitioning into CRs were sampled from recovering roots of grafted plants. Expression analysis revealed that *LBD16*, *NIN,* and *NF-YA* genes were upregulated in wild-type rootstocks when *ccr1* mutants were used as scions, independently of symbiotic interactions, clearly demonstrating a systemic regulation of these genes by AoDev (Fig. 6*D*). To further investigate the P nutritional response, a transcriptomic dataset comparing wild-type plants under P-rich and P-deficient conditions was analyzed (Dataset S9). Differential expression analysis [Absolute Log2(fold change) > 2 and FDR < 0.05], followed by a GO enrichment analysis revealed two significantly enriched biological processes: "cellular response to phosphate starvation" and "dephosphorylation," validating the robustness of the dataset (Dataset S10). The downstream AoDev pathway, including *TML, NIN, LBD16,* and *NF-YA* genes, showed weak responsiveness in response to P (*SI Appendix*, Fig. S8*A* and Dataset S11). However, specific qPCR analysis of miRNAs revealed a more pronounced downregulation of *miR2111c* under P-rich conditions (*SI Appendix*, Fig. S8*B*).

Analysis of the *L. albus* CLE Prepropeptide Gene Family. To gain insights into the root-to-shoot signal of AoDev, a comprehensive reannotation of CLE prepropeptides in *L. albus* was performed using the NCBI BLASTp tool and the *M. truncatula* genome, identifying 70 sequences that were categorized into the seven previously established CLE groups (29, 30) (*SI Appendix*, Fig. S9). Several *L. albus* peptides clustered within Group VI, including Lalb_Chr01g0005951 with MtCLE12 and Lalb_Chr01g0016681 and Lalb_Chr25g0286011 with MtCLE35. These *Medicago* peptides, MtCLE12 and MtCLE35, are typically induced by rhizobia and associated with AoN. The phylogenetically related *L. albus* peptides were not expressed in either wild-type or *ccr1-1* mutant plants, consistent with the absence of rhizobium inoculation under the experimental conditions (Datasets S7 and S12). In contrast, five CLE peptide genes were significantly upregulated (Log2(fold change) > 3), in the *ccr1-1* mutant compared to wild-type plants (Fig. 6*C*). Notably, four of these genes were classified within Group VII, while one was assigned to Group VI/VII (Dataset S12). Among the Group VII genes, *Lalb_Chr01g0006711* and *Lalb_Chr19g0133921* also displayed upregulation during CR development [Log2(fold change) > 2], as evidenced by the developmental transcriptome analysis (Fig. 6*B* and Dataset S12). For these two CLE genes, the upregulation in *ccr1* background was further confirmed in another *ccr1* allele (*ccr1-2*) through RT-qPCR analysis (*SI Appendix*, Fig. S7*C*). While none of the 70 *L. albus* CLE prepropeptide genes exhibited a strong differential expression in response to P availability, *Lalb_Chr01g0006711* and *Lalb_Chr19g0133921* displayed a modest but significant induction under P-rich conditions (*SI Appendix*, Fig. S8 and Dataset S12). These two CLE peptides are thus upregulated across the three transcriptomic datasets analyzed: in *ccr1* background, in developing rootlets, and under P-rich conditions. A Salmon-based quantification of the NCBI BioProject PRJNA394259 transcriptomic dataset for *L. albus* nodules in symbiosis with *Bradyrhizobium japonicum* and *Bradyrhizobium valentinum* (31) detected no expression of these CLE prepropeptide genes in the nodules (Dataset S13). This result supports a specificity of these peptides as negative regulators of CR development. Interestingly, they phylogenetically cluster with MtCLE53, a mycorrhiza-induced peptide known as a negative regulator of arbuscular mycorrhiza symbiosis (*SI Appendix*, Fig. S9).

Discussion

In our effort to identify regulatory mechanisms governing cluster root (CR) development in white lupin, we performed a forward genetic screen, uncovering four allelic *ccr1* mutants that constitutively produce CRs even under repressive conditions, such as high phosphate (P) availability. Independent mapping of these 4 mutants identified *LalbCCR1* as the gene responsible for inhibiting CR development in wild-type plants. Due to previous genome polyploidization events in white lupin, most gene families contain multiple members, suggesting the existence of *CCR1-like* genes. We identified a single close paralog, but sequence analysis revealed a G > E substitution similar to those found in the *ccr1-1* and *ccr1-3* mutants, indicating that this paralog is nonfunctional. The absence of genetic redundancy within the *CCR1* gene family likely contributed to the success of our genetic screen.

The strong synteny between *LalbCCR1* locus and *MtSUNN*, *LjHAR1,* and *GmNARK* loci suggests that *LalbCCR1* is the ortholog of the well-characterized *CLV1-like LRR-RLK*s which control AoN. This prompted us to investigate whether *ccr1* mutants are also affected in nodulation, pointing to a common regulatory mechanism governing both nodule formation and cluster root development. Both the *ccr1-1* and *ccr1-2* alleles displayed hypernodulation phenotypes, similar to *har1*, *sunn,* or *nark* mutants. Moreover, grafting experiments confirmed the systemic nature of this nodule regulation. To investigate CR development, additional grafting experiments were performed, which revealed that CR formation is also controlled systemically via a shoot-to-root *LalbCCR1* signaling cascade. Under P-rich conditions, *ccr1* shoots (from both *ccr1-1* and *ccr1-2* mutants) allowed the development of excessive number of CRs in wild-type rootstocks. These findings demonstrate the presence of a shared inhibitory pathway that regulates both nodule and CR organogenesis in lupin, leading us to conclude that *LalbCCR1* functions as a negative long-distance regulator of these two developmental processes.

Interspecific grafting between WL and NLL highlighted that the inhibitory *LalbCCR1* pathway is not specific to WL but is conserved across at least these two lupin species. Interestingly, a dose-dependent effect in grafting phenotypes reveals that the strength of this inhibition correlates with the number of functional *CCR1* paralogs (*CCR1* and *CCR1*-like). The inhibitory effect exerted by NLL shoots on *ccr1* rootstocks is particularly striking and significantly stronger than that of WL shoots, in which the *CCR1-like* paralog is mutated and nonfunctional. This observation suggests that the presence of a strong systemic inhibition signal may be the underlying mechanism for the lack of CRs in NLL. Further experiments are required to characterize the nature of this inhibitory signal, with current evidence pointing to the involvement of mobile miRNAs and hormones, such as cytokinins, as seen in model legumes (32). Whether these signals are conserved across all legumes and beyond remains an open question.

Our transcriptome analyses revealed that several developmental genes are upregulated in *ccr1* mutants, some of which are also involved in CR formation and are orthologs of lateral root (LR) development genes, such as *LDB16, WOX5,* and *PLT* (33). Recent evidence indicates that elements of the LR developmental program are co-opted into the root nodule development pathway in legumes (34, 35). The Nodule Inception (NIN) transcription factor plays a pivotal role in this integration by modulating the expression of both *LBD16* and *NF-YA* genes (36, 37). Consistent with these data, we observed upregulation of *NIN* and *NF-YA* genes in *ccr1* mutants, even in the absence of rhizobial infection or nodule organogenesis. These transcriptional changes suggest that *LalbCCR1* targets the *NIN/LBD16-NFYA* module, which controls both root and nodule organogenesis. Further grafting experiments and RT-qPCR analysis demonstrated that the up-regulation of the *NIN/LBD16-NFYA* module operates systemically. Only late symbiotic genes, likely associated with developmental processes, were upregulated in *ccr1*, whereas early symbiotic genes, primarily involved in signaling, remained unchanged. These findings suggest that *CCR1* does not influence the symbiotic dialogue between the two symbiotic partners but rather imposes its inhibitory effect specifically on the developmental stage of nodulation.

Historically, LRR-RLKs involved in AoN have been shown to regulate both nodulation and root architecture in model legumes (8, 9, 11, 24, 38). However, LRR-RLKs involved in AoN are expressed in both shoots and roots, and while nodule development is widely accepted to be under systemic negative regulation, root development appears to be primarily controlled by local mechanisms. For example, the CEP1/MtCRA2 module, which systemically regulates nodulation in *Medicago*, has been shown to control root development locally (13, 38). The same results have been reported for the MtCLE35/SUNN module (39). Recent split-roots experiments in white lupin also suggest a local role for a LalbCLE35 root peptide in regulating rootlet density and length (40). However, our results provide clear evidence that the development of CR is under systemic control through the shoot-to-root *LalbCCR1* pathway, although the additional contribution of local regulatory mechanisms cannot be ruled out. Given that *LalbCCR1* regulates both nodule and CR development via a systemic signaling pathway, we propose the term AoDev to describe this mechanism. This term emphasizes the plant's capacity to limit the development of root energy-intensive organs, whether symbiotic or nonsymbiotic, optimizing resource allocation between nutrient acquisition and carbon expenditure.

To explore the root-to-shoot pathway of AoDev, a preliminary analysis of the *L. albus* CLE prepropeptide family revealed that genes upregulated in the *ccr1-1* mutant compared to the wild type predominantly belong to Group VII, as classified by Hastwell et al. (29, 30). Notably, four of these genes (*Lalb_Chr01g0006711, Lalb_Chr01g0006721, Lalb_Chr09g0327981,* and *Lalb_Chr19g0133921)* clustered phylogenetically with *M. truncatula* CLE53 (*MtCLE53)*, a mycorrhizal-induced gene known to negatively regulate arbuscular mycorrhizal (AM) colonization (41). Among these, *Lalb_Chr01g0006711* and *Lalb_Chr19g0133921* were also upregulated during the transition of LR to CR. These results suggest a potential role for these CLE peptides in the autoregulation of CR development mediated by *LalbCCR1* through a negative feedback mechanism controlling CR development, analogous to the regulation observed in AM symbiosis. Interestingly, although species in the *Lupinus* genus have lost the ability to form AM symbiosis, the regulators of CR development appear to be evolutionarily related to those involved in AM regulation. While this study did not specifically investigate P responses, it is noteworthy that Group VII includes several MtCLE genes identified as P-inducible (*MtCLE33*, *MtCLE34*, *MtCLE42,* and *MtCLE43*) (41). Among the 70 LalbCLE peptides, none were found to be strongly P-inducible; however, *Lalb_Chr01g0006711* and *Lalb_Chr19g0133921* displayed modest but significant induction under P-rich conditions. Notably, these two CLE peptides demonstrated consistent upregulation across three key contexts: i) the *ccr1-1* mutant background, ii) CR development and iii) P-rich conditions. Furthermore, they are not detected in nodules. These findings position them as potential CR-specific negative regulators of development governing the root-to-shoot signaling mechanism of the AoDev. Overall, this study has identified several *LalbCLE* peptide genes that warrant further investigation to achieve a comprehensive functional characterization of the *LalbCCR1*-mediated mechanism regulating both nodule and CR development.

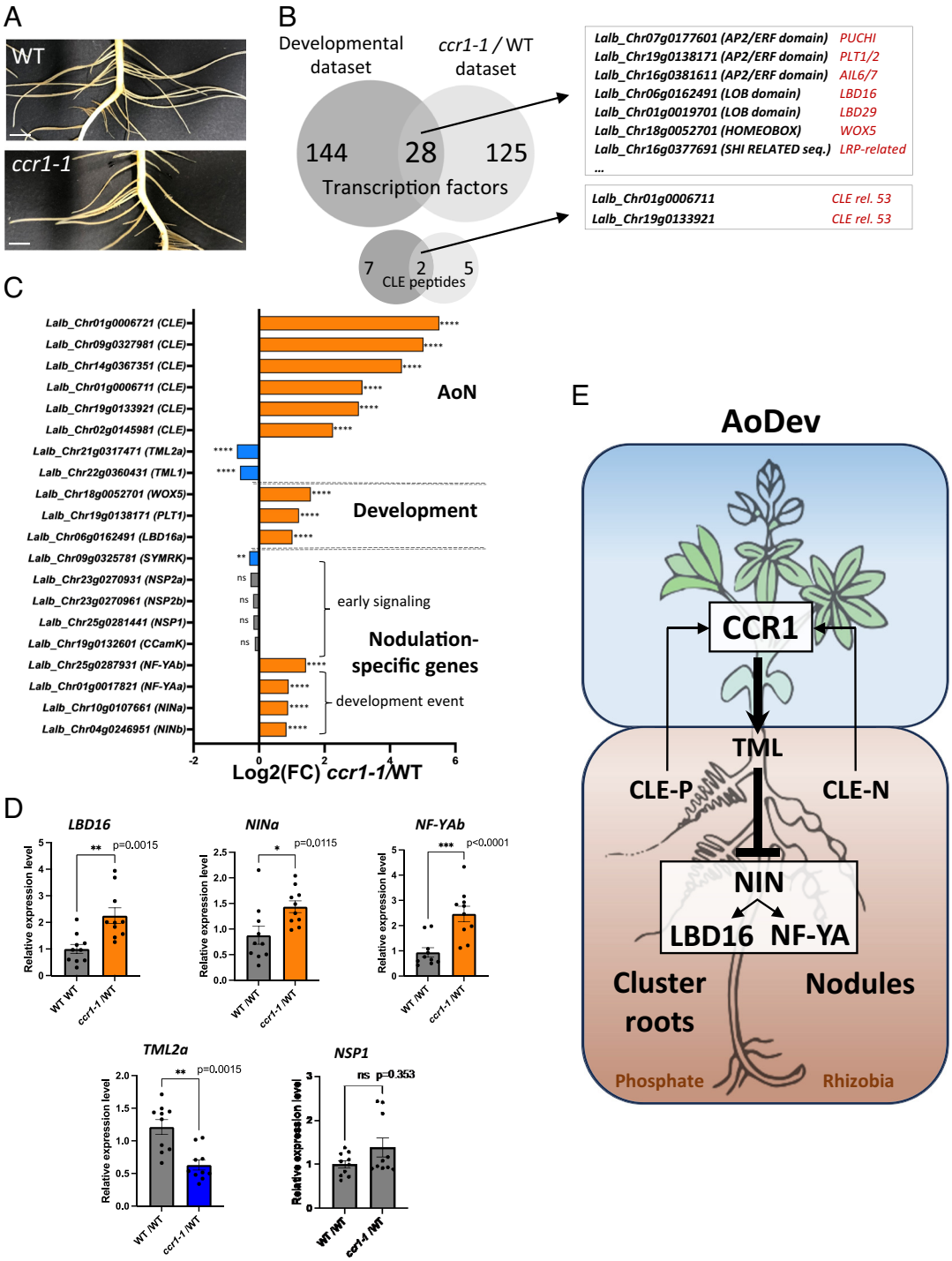

Fig. 6. Transcriptional expression analysis of genes deregulated in *ccr1-1* mutant and during CR development in transcriptomic datasets and rootstocks of grafted plants, leading to the proposed model of the systemic AoDev pathway. (*A*) Illustrations depicting the developmental stages of roots used for sampling the LRs from WT and *ccr1-1* plants for the RNAseq. LRs longer than 3 cm from three plants were pooled, and four biological replicates were collected. (Scale bar, 1 cm.) (*B*) Venn diagrams illustrating the overlap of transcription factors-encoding genes upregulated in the developmental transcriptomic dataset (T024-036-048 /LR) [Absolute Log2(fold change) > 2, FDR < 0.05] compared to those upregulated in the *ccr1-1* CR/wild-type transcriptomic dataset [Absolute Log2(fold change) > 1, FDR < 0.05] and the overlap of CLE prepropeptide genes upregulated in the developmental transcriptomic dataset (T024-036-048/LR) [Absolute Log2(fold change) > 2, FDR < 0.05] compared to those upregulated in the *ccr1-1* CR /wild-type transcriptomic dataset (Absolute Log2(fold change) > 3, FDR < 0.05). Normalization and differential expression analysis were performed using the DIANEbeta R package (28). (*C*) Differential expression analysis of selected key genes in the *ccr1-1* mutants relative to wild-type plants, focusing on AoN, CR development, and nodulation genes. Expected regulations were observed for AoN genes with up-regulation of *CLE* genes and down-regulation of *TML* genes, compared to wild-type. Transcription factors such as *LBD16, WOX5,* and *PLT1/2* involved in lateral root development were significantly up-regulated in *ccr1-1* mutant. Early nodulation genes were not significantly deregulated in *ccr1-1* mutant, whereas *NIN* and *NF-YA* genes were significantly up-regulated. Fold changes and adjusted *P*-values (FDR) were calculated using DIANEbeta R package (28); ns *P*-adjust > 0.05, **P*-adjust < 0.05, ***P*-adjust < 0.01, ****P*-adjust < 0.001, *****P*-adjust < 0.0001. (*D*) RT-qPCR analysis of the expression levels of selected genes in wild-type rootstocks of grafted plants using either wild-type (WT/WT) or *ccr1-1* mutants (*ccr1-1*/WT) as scions. The grafting experiment revealed that *LBD16*, *TML*, *NIN*, and *NF-YA* genes are systemically regulated by *LalbCCR1* via a shoot-to-root signaling pathway, whereas *NSP1* is not differentially regulated. The experiment validated the regulatory pattern observed in the transcriptomic data and provides compelling evidence for the existence of a systemic pathway. Error bars represent mean ± SE, and statistical analysis was performed using two-tailed Mann–Whitney tests: ns *P*-value > 0/05, **P*-value < 0.05, ***P*-value < 0.0, ****P*-value < 0.00, *****P*-value < 0.0001. (*E*) Proposed model for the AoDev pathway, depicting a systemic root-to-shoot-to-root signaling mechanism involving the LRR-RLK LalbCCR1, which represses the *NIN/LBD16/NF-YA* module, leading to the inhibition of both CR and nodule development.

A key question arising from this work is how nitrate (N) and phosphate (P) sensing pathways are integrated to control both nodule and cluster root development (42). These regulations likely involve a complex interplay of local and systemic control mechanisms, with different peptide/LRR-RLK module contributions. While we have identified the AoDev pathway as a dominant systemic regulatory force in legumes, similar to the previously characterized AoN pathway (43), local-level regulations also exist. Indeed, in nonlegumes, LRR-RLK signaling pathways are increasingly recognized as key regulators of root system architecture in response to environmental conditions, with most studies emphasizing local regulatory processes (44–46). In *Arabidopsis thaliana,* the closest homolog of HAR1/NARK/SUNN/CCR1 is CLV1, which has been implicated in regulating lateral root development in low nitrogen conditions (47). However, whether this regulation operates at a local or a systemic level, remains unresolved. Additionally, N and P availability are expected to control nodulation and cluster root formation. Previous studies have shown that white lupin grown under P-deficient conditions produced significantly more nodules than in P-rich conditions, while total nodule mass remained unchanged (48). This suggests that nodule initiation is increased under P-deficient conditions, but secondary regulatory mechanisms constrain their subsequent growth. Overall, these results support our hypothesis that nodule and CR development share AoDev as a common negative regulatory pathway acting during the early developmental stages of both organs under P-rich conditions. Importantly, AoDev also exerts a negative feedback control on nodule and CR numbers under P-deficient conditions, likely to optimize energy allocation of the roots. Our findings provide a foundation for understanding the AoDev as a systemic, ancestral pathway that modulates root system architecture. This pathway likely represents a crucial nexus between shoot carbon fixation and root mineral nutrition, offering insights into how plants integrate above- and below-ground processes to optimize resource allocation, nutrition, and development.

Materials and Methods

Plant Material and Cultivation. White lupin (*L. albus*) cv. AMIGA (Florimond Desprez, France) and narrow-leaved lupin (*L. angustifolius*) cv. TANJIL (CSIRO, Australia) were used in this study. Seeds were germinated on a vermiculite substrate for 4 d, after which they were cultivated in 200 L hydroponic tanks containing the following well-aerated nutritive solution: 400 µM $Ca(NO_3)$, 54 µM $MgSO_4$, 0.24 µM $MnSO_4$, 0.1 µM $ZnSO_4$, 0.018 µM $CuSO_4$, 2.4 µM H_3BO_3, 0.03 µM Na_2MoO_4, 10 µM Fe-EDTA, and either 200 µM K_2SO_4 for phosphate-deficient (−P) or 400 µM of KH_2PO_4 for phosphate-rich (+P) experiments. Growth chambers are set to a photoperiod of 16 h light/8 h dark, 25 °C day/20 °C night, 65% relative humidity, and photon flux density of 200 µmol m^{-2} s^{-1}.

Grafting experiments were conducted at 7 d postgermination. The scion was prepared by trimming to a V-shape and inserted into a vertical slit created in the rootstock. Postgrafting, root recovery rates ranged from 20 to 60% over the subsequent 3 to 7 d, contingent to the specific scion–rootstock pairing. Phenotyping analyses were conducted on 20-d-old plants. The number of LRs exhibiting clusters of rootlets, referred to as CR in this study, was counted. Measurements of primary and LR lengths, as well as root dry weight, were also measured. Data were plotted and statistically analyzed using GraphPad Prism software 10.2. In order to visualize physiological activities of *ccr1-1* root systems, roots were spread on 0.8% agar plates containing either, 0.005% (m/v) bromocresol purple buffered in Tris-HCl pH 6 for testing proton excretion, or 0.013% (m/v) 5-Bromo-4-chloro-3-indolyl phosphate-buffered in sodium acetate pH 5 for testing phosphatase activity, or 330 µM bathophenanthroline disulfonic acid disodium salt, 100 µM FeNaEDTA for testing ferric reductase activity.

EMS Population and Genetic Screen. A large-scale mutagenesis was conducted on AMIGA seeds using 0.4% ethyl methanesulfonate (EMS) for 3 h and deactivation with sodium thiosulfate 2.5% for 5 min. M1 seedlings were subsequently cultivated in the Cerience experimental fields (Poitiers, France) and the pods from each individual M1 plant were harvested, resulting in an EMS-mutagenized population of 5,000 M2 batches. Finally, 36 seeds from each of 800 M2 batches were screened in P-rich medium to identify plants exhibiting constitutive cluster roots. Plants with the same constitutive cluster root phenotype were found in 4 independent batches and amplified. They were crossed for allelic test and back-crossed with AMIGA for the mapping by sequencing strategy. Pools of 50 to 90 F2 plants with a mutant phenotype (homozygous) and similarly sized pools of plants with a wild-type phenotype (WT batch) were harvested for DNA extraction and sequencing by Illumina HiSeq at Get-PlaGe core facility (INRAe, Toulouse, France). A mean coverage of 50× to 100× was obtained across samples. Cutadapt v1.15 (49) has been used to remove Illumina TruSeq adapter from the sequencing data and to remove bases with a quality score lower than 20, in both 5′ and 3′ ends of the reads. Pairs of reads containing one read with a length lower than 35 have been discarded. We used BWA-MEM v0.7.17 (50) to map reads to the white lupin reference genome. Picard MarkDuplicates v2.20.1 (https://github.com/broadinstitute/picard) has been used to detect and remove PCR and Optical duplicates. We then used GATK HaplotypeCaller v4.1.4.1 (49) tool to call variants and snpEff 4.3t (50) to annotate them. The duplicate free mapped reads have been used as input for the MutMap pipeline v2.1.2 (51).

Microscopy. Root segments transitioning to CR were fixed with 4% paraformaldehyde for 120 min at room temperature under vacuum treatment and then washed twice for 2 min in 1X PBS before being embedded in 3% (w/v) agarose resin in PBS. Longitudinal root sections of 100 µm were cut with a vibrating microtome (Microcut H1200, BioRad). The sections were stained with 2 µg/mL 4,6 diamidino-2-phenylindole (DAPI). Fluorescence was observed using a ZEISS Axio Observer microscope, with a plan-apochromatic 20X/0.8 objective and the following filters: BP 325-390 nm for excitation and BP 445/50 for emission. Mosaic pictures were taken using the Apotome module. Images were captured with OrcaFlash (Hamamatsu) controlled with the ZEISS Zen blue Software. In nodulation experiments, nodules were observed in dark field with the OLYMPUS SZX16 stereo microscope, and images were taken with a DP72 camera.

Structural and Phylogenetic Analysis. AlphaFold structure prediction was performed using ColabFold v1.5.5: AlphaFold2 with MMseqs2 (52, 53), providing the amino acid sequence of LalbCCR1 (*LalbChr03g0025491*). PyMol v2.5.4 was used to visualize and modify the protein structure to make the transmembrane domain apparent, and to indicate the positions of amino acid substitutions within the structure. Closest LalbCCR1 homologs from white lupin, narrow-leaved lupin, *Glycine max*, *Lotus japonicus*, *M. truncatula,* and *Arabidopsis thaliana* were retrieved using NCBI BLASTp tool. Alignment of the kinase domain portion was conducted using MUSCLE (54) alignment software on the NGPhylogeny website with default settings, and the alignment output was refined with JalView 2.11.3.3 (55). Due to inaccuracies in the original annotation, CLE prepropeptide genes were reannotated in detail using the NCBI BLASTp tool against *M. truncatula* genes. Phylogenetic analysis was performed using the PhyML/OneClick workflow on NGPhylogeny with default parameters (56). The resultant phylogenetic trees were generated using iTOl v6 (57). Synteny analysis utilized genome assemblies from *M. truncatula* A17 r5.0 (58), *G. max* Williams 82 v4.0 (59), *L. japonicus* MG20 v3.0 (60) and *L. albus* v1.0 (61). It was carried out using Easyfig 2.2.5 (62) with BLASTn and a minimum identity value for the BLAST at 0.7. The output of Easyfig was subsequently edited with Inkscape 1.2.1.

Nodulation Assays. For nodulation experiments, plants were grown in Magenta GA-7 pot filled with leached and sterilized zeolite substrate (Siliz 14, Somez, France) supplied with a nutrient solution corresponding to the previously described P-rich medium but without nitrogen. Seeds were sterilized with calcium hypochlorite, germinated in Petri dishes, and then transferred into Magenta pots. The *Bradyrhizobium lupini* MIAE428 strain (previously named LL13) (63) was used. Inoculum was produced by cultivating the strain in modified yeast mannitol (YM) medium (mannitol 10 g/L, yeast extract 1 g/L, K_2HPO_4 0.5 g/L, NaCl 50 mg/L magnesium sulfate $7H_2O$ 100 mg/L, calcium chloride 40 mg/L, glutamic acid 0.43 g/L, $FeCl_3$ 4 mg/L) supplemented with nalidixic acid 20 µg/L, in the dark for 4 d at 28 °C. One mL inoculum was applied one week after the seedlings were transferred to the pots or one week after grafting. Nodule numbers per plant were assessed and the leaf chlorophyll content was indirectly estimated using a

Chlorophyll meter SPAD (Konica-Minolta) on the third youngest leaf. Data were plotted and statistically analyzed using GraphPad Prism software 10.2.

Gene Expression Analysis. Developmental temporal transcriptome. The sampling began (T0) on eight-day-old plants grown under P-deficient conditions. A total of eight 1 cm-long transitioning CR segments from four independently grown plants was sampled, at a distance of 1 cm from the primary root, in the upper part of the root system where LRs are transitioning to CR, every 12 h for 5 d, covering the entire rootlet developmental process (T0 to T132). As a control, 1 cm-long lateral root segments not transitioning to CR were collected. Four biological replications were produced for each experiment. Total RNA was extracted from all frozen samples using the Direct-zol RNA MiniPrep kit (Zymo Research) according to the manufacturer's recommendations. A total of 52 independent root RNA-seq libraries were constructed and sequenced at the Get-PlaGe core facility (INRAe, Toulouse, France). The Illumina TruSeq Stranded mRNA Sample Preparation Kit (Illumina Inc.) was used according to the manufacturer's protocol. Paired-end sequencing was performed, generating 2 × 150 bp reads using TruSeq SBS kit v3 sequencing chemistry on an Illumina NovaSeq instrument. Raw reads were cleaned using Cutadapt v1.15 (64), by removing bases with a quality score lower than 30, in both 5′ and 3′ ends of the reads, as well as TruSeq Illumina adapters. Pairs of reads containing one read with a length lower than 35 have been discarded. The quality-checked RNA-seq reads were mapped on the white lupin genome reference using Hisat2 v2.1.0, with the following parameters "--rna-strandness RF --dta". Transcripts were assembled and quantified using Stringtie v1.3.4d with the options "--rf -e -B -u -M 1".

ccr1-1 mutant transcriptome. All LRs of four ten-day-old plants grown in P-deficient conditions were harvested from the upper part of the root system, corresponding to the zone where LRs are transitioning to CR. Eight independent RNA-seq libraries were constructed and processed as described for developmental transcriptome.

Phosphate response transcriptome. Whole root systems of ten-day-old wild-type AMIGA plants grown in phosphate-rich (500 µM H_2PO_4) or in the absence of phosphate were harvested. Four biological replicates were produced for each condition. Two independent RNA-seq libraries were constructed and processed as above. Two sequencing lines for each replicate were produced.

Normalization, differential expression, and gene ontology enrichment analysis were performed using the DIANEbeta R package (28) (https://shinyapps.southgreen.fr/app/dianebeta) v1.1.0.1. The TCC R package with the "tmm" normalization method was used, with prior removal of differentially expressed genes. For each analysis, Log2(fold change) and false discovery rate–adjusted *P*-value (FDR) were provided in the text and figure legends. SRPlot online (65) was used for generating the PCA, heatmap, and the GO plots, and GraphPad Prism software 10.2 for the statistical analysis and kinetic expression data plotting. The GO terms used for enrichment are available for download at https://www.whitelupin.fr/download.html.

RT-qPCR Experiments. For *LalbCCR1* expression in different organs, 12-d-old plants grown under either P-deficient or P-rich conditions were sampled. Samples included for lateral roots (LR), root apical meristem (RAM), shoot apical meristem (SAM), leaf, petiole, and hypocotyl. Cluster root (CR) samples were collected exclusively from plants grown on P-deficient conditions. CRs were collected from the upper part of the root system, while LRs were collected below. The apices of LR and CR were removed. Petioles and leaves were collected from the second leaf. Each sample contained tissues from 3 individual plants and 3 biological replicates were collected for each plant part. For experiments confirming RNA-seq data in another allele besides *ccr1-1*, samples were collected from the root system of *ccr1-2* mutant plants following the same protocol as for the RNA-seq study. For the grafted plants, this protocol was applied to roots recovering after the grafting operation. At least five biological replicates were collected and analyzed in each experiment. Total RNA was extracted using the Direct-zol RNA MiniPrep kit (Zymo Research) according to the manufacturer's recommendations. RNA concentration was measured on a NanoDrop (ND1000) spectrophotometer. Poly(dT) cDNAs were synthesized from 2 µg total RNA using the RevertAid First Strand cDNA Synthesis (ThermoFisher). For miRNA expression analysis, gene-specific RT primers were used for stem-loop cDNA synthesis using miR168a as normalizer. Gene expression was measured by quantitative Real Time-PCR (qRT-PCR) (LightCycler 480, Roche Diagnostics) using the SYBR Premix Ex Taq (Tli RNaseH, Takara, Clontech). Expression levels were normalized to a putative initiation factor *LalbEIF-4* (*Lalb_Chr07g0195211*) or to a *LalbPolyubiquitin* (*Lalb_Chr06g0164891*). Two technical replicates were performed for all qRT-PCR experiments. Specific primer pairs are described in Dataset S14. Relative gene expression levels were calculated according to the ΔΔCt method, using LR, for organ expression, or WT and WT/WT, samples for *ccr1-2* and grafted plants respectively.

Data, Materials, and Software Availability. RNAseq raw reads data have been deposited in NCBI [https://dataview.ncbi.nlm.nih.gov/object/PRJNA1124865?reviewer=851s8ptss62fl7h178k2j5f8bu (66); https://dataview.ncbi.nlm.nih.gov/object/PRJNA1125199?reviewer=m1lhh43j385of3s7hgrnsd7ucp (67); https://dataview.ncbi.nlm.nih.gov/object/PRJNA1198000?reviewer=4m291qtjeonrvbsqdk7n5qipg5FASTQ (68) raw sequence files are available at NCBI under the Bioproject number PRJNA1124865 for the developmental temporal RNAseq (Sequence Read Archive accession numbers SAMN41865670-82), number PRJNA1125199 for the ccr1-1 RNAseq (SRA accession numbers SRR29446565-79) and number PRJNA1198000 (SRA accession numbers SAMN45825493-508) for the phosphate response RNAseq.].

ACKNOWLEDGMENTS. We thank Nathalie Harzic (Cerience, Poitiers) for the white lupin EMS mutagenesis and agricultural support. We thank Carine Alcon from the PHIV facility (Plateforme d'Histocytologie et d'Imagerie cellulaire Végétale of IPSiM lab) for her valuable comments and technical assistance with microscopy imaging. We thank Cécile Revellin (UMR Agroécologie, INRAE Dijon) for the gift of MIAE428 *Bradyrhizobium lupini* strain. We also wish to thank Valérie Hocher and Darius T. Nzepang (IRD, Montpellier) for technical help in setting up nodulation protocols for white lupin. We thank Lars Kamphuis and Karam Singh (CSIRO, Australia) for providing narrow-leafed lupin TANJIL seeds. We thank Willy Aubert (CNRS, Montpellier) and Soledad Traubenik (IPS2, Saclay) for their technical help on miRNA expression studies. This project has received funding from the European Research Council (ERC) under the European Union's Horizon 2020 research and innovation program (Starting Grant LUPINROOTS–Grant agreement No 637420 to B.P.). This project was supported by the French ANR (ANR-19-CE13-0029 MicroLUP to B.P.). We thank CNRS Biologie for the Diversity of Biological Mechanisms Grant support to L.M. We also thank INRAE Département BAP for its support to E.I.

Author affiliations: [a]Institute for Plant Sciences of Montpellier, Univ Montpellier, Centre National de la Recherche Scientifique, Institut National de Recherche pour l'Agriculture, l'Alimentation et l'Environnement, Institut Agro, Montpellier 34060, France

Author contributions: L.M., B.H., and B.P. designed research; L.M., F.D., A.B., F.G., C.M.-C., V.F., I.V., E.I., and B.H. performed research; L.M., A.S., H.P., B.H., and B.P. analyzed data; and L.M. and B.P. wrote the paper.

The authors declare no competing interest.

This article is a PNAS Direct Submission.

1. S. Ruffel *et al.*, Nitrogen economics of root foraging: Transitive closure of the nitrate–cytokinin relay and distinct systemic signaling for N supply vs. demand. *Proc. Natl. Acad. Sci. U.S.A.* **108**, 18524–18529 (2011).
2. Z. Jia, N. von Wirén, Signaling pathways underlying nitrogen-dependent changes in root system architecture: From model to crop species. *J. Exp. Bot.* **71**, 4393–4404 (2020).
3. Y. Ohkubo, M. Tanaka, R. Tabata, M. Ogawa-Ohnishi, Y. Matsubayashi, Shoot-to-root mobile polypeptides involved in systemic regulation of nitrogen acquisition. *Nature Plants* **3**, 1–6 (2017).
4. B. W. Jeon *et al.*, Recent advances in peptide signaling during Arabidopsis root development. *J. Exp. Bot.* **72**, 2889–2902 (2021).
5. G. Caetano-Anollés, P. M. Gresshoff, Plant genetic control of nodulation. *Annu. Rev. Microbiol.* **45**, 345–382 (1991).
6. E. Oka-Kira, M. Kawaguchi, Long-distance signaling to control root nodule number. *Curr. Opin. Plant Biol.* **9**, 496–502 (2006).
7. Y. Li *et al.*, Progress in the Self-regulation system in legume nodule development-AON (autoregulation of nodulation). *Int. J. Mol. Sci.* **23**, 6676 (2022).
8. R. Nishimura *et al.*, HAR1 mediates systemic regulation of symbiotic organ development. *Nature* **420**, 426–429 (2002).
9. L. Krusell *et al.*, Shoot control of root development and nodulation is mediated by a receptor-like kinase. *Nature* **420**, 422–426 (2002).

10. I. R. Searle *et al.*, Long-distance signaling in nodulation directed by a CLAVATA1-like receptor kinase. *Science* **299**, 109–112 (2003).
11. E. Schnabel, E.-P. Journet, F. de Carvalho-Niebel, G. Duc, J. Frugoli, The Medicago truncatula SUNN gene encodes a CLV1-likeLeucine-rich repeat receptor kinase that regulates nodule number and root length. *Plant Mol. Biol.* **58**, 809–822 (2005).
12. C. Laffont *et al.*, Independent regulation of symbiotic nodulation by the SUNN negative and CRA2 positive systemic pathways. *Plant Physiol.* **180**, 559–570 (2019).
13. N. A. Mohd-Radzman *et al.*, Novel MtCEP1 peptides produced in vivo differentially regulate root development in Medicago truncatula. *J. Exp. Bot.* **66**, 5289–300 (2015).
14. D. Tsikou *et al.*, Systemic control of legume susceptibility to rhizobial infection by a mobile microRNA. *Science* **362**, 233–236 (2018).
15. M. Takahara *et al.*, Too much love, a novel Kelch repeat-containing F-box protein, functions in the long-distance regulation of the legume–Rhizobium symbiosis. *Plant Cell Physiol.* **54**, 433–447 (2013).
16. P. Gautrat *et al.*, Unraveling new molecular players involved in the autoregulation of nodulation in Medicago truncatula. *J. Exp. Bot.* **70**, 1407–1417 (2019).
17. G. Neumann, E. Martinoia, Cluster roots–an underground adaptation for survival in extreme environments. *Trends Plant Sci.* **7**, 162–167 (2002).
18. L. Cheng *et al.*, White lupin cluster root acclimation to phosphorus deficiency and root hair development involve unique glycerophosphodiester phosphodiesterases. *Plant Physiol.* **156**, 1131–48 (2011).
19. M. Watt, J. R. Evans, Proteoid roots. Physiology and development. *Plant Physiol.* **121**, 317–24 (1999).
20. A. Massonneau *et al.*, Metabolic changes associated with cluster root development in white lupin (Lupinus albus L.): Relationship between organic acid excretion, sucrose metabolism and energy status. *Planta* **213**, 534–42 (2001).
21. T. Le Thanh *et al.*, Dynamic development of white lupin rootlets along a cluster root. *Front. Plant Sci.* **12**, 738172 (2021).
22. K. R. Skene, Pattern formation in cluster roots: Some developmental and evolutionary considerations. *Ann. Bot.* **85**, 901–908 (2000).
23. B. Hufnagel *et al.*, Pangenome of white lupin provides insights into the diversity of the species. *Plant Biotechnol. J.* **19**, 2532–2543 (2021).
24. J. Wopereis *et al.*, Short root mutant of Lotus japonicus with a dramatically altered symbiotic phenotype. *Plant J.* **23**, 97–114 (2000).
25. B. J. Carroll, D. L. McNeil, P. M. Gresshoff, A supernodulation and nitrate-tolerant symbiotic (nts) soybean mutant. *Plant Physiol.* **78**, 34–40 (1985).
26. C. Gallardo *et al.*, Anatomical and hormonal description of rootlet primordium development along white lupin cluster root. *Physiol. Plant.* **165**, 4–16 (2019).
27. U. Voß *et al.*, The circadian clock rephases during lateral root organ initiation in Arabidopsis thaliana. *Nat. Commun.* **6**, 7641 (2015).
28. O. Cassan, S. Lèbre, A. Martin, Inferring and analyzing gene regulatory networks from multi-factorial expression data: A complete and interactive suite. *BMC Genomics* **22**, 387 (2021).
29. A. H. Hastwell, P. M. Gresshoff, B. J. Ferguson, Genome-wide annotation and characterization of CLAVATA/ESR (CLE) peptide hormones of soybean (Glycine max) and common bean (Phaseolus vulgaris), and their orthologues of Arabidopsis thaliana. *J. Exp. Bot.* **66**, 5271–5287 (2015).
30. A. H. Hastwell, T. C. de Bang, P. M. Gresshoff, B. J. Ferguson, CLE peptide-encoding gene families in Medicago truncatula and Lotus japonicus, compared with those of soybean, common bean and Arabidopsis. *Sci. Rep.* **7**, 9384 (2017).
31. J. Keller *et al.*, RNA sequencing and analysis of three Lupinus nodulomes provide new insights into specific host-symbiont relationships with compatible and incompatible Bradyrhizobium strains. *Plant Sci.* **266**, 102–116 (2018).
32. C. Concha, P. Doerner, The impact of the rhizobia–legume symbiosis on host root system architecture. *J. Exp. Bot.* **71**, 3902–3921 (2020).
33. T. Goh *et al.*, Lateral root initiation requires the sequential induction of transcription factors LBD16 and PUCHI in Arabidopsis thaliana. *New Phytol.* **224**, 749–760 (2019).
34. T. Soyano, M. Liu, M. Kawaguchi, M. Hayashi, Leguminous nodule symbiosis involves recruitment of factors contributing to lateral root development. *Curr. Opin. Plant Biol.* **59**, 102000 (2021).
35. M. Lebedeva, M. Azarakhsh, D. Sadikova, L. Lutova, At the root of nodule organogenesis: Conserved regulatory pathways recruited by rhizobia. *Plants* **10**, 2654 (2021).
36. T. Soyano, Y. Shimoda, M. Kawaguchi, M. Hayashi, A shared gene drives lateral root development and root nodule symbiosis pathways in Lotus. *Science* **366**, 1021–1023 (2019).
37. K. Schiessl *et al.*, Nodule inception recruits the lateral root developmental program for symbiotic nodule organogenesis in medicago truncatula. *Current Biol.* **29**, 3657–3668.e5 (2019).
38. E. Huault *et al.*, Local and systemic regulation of plant root system architecture and symbiotic nodulation by a receptor-like kinase. *PLoS Genet.* **10**, e1004891 (2014).
39. M. A. Lebedeva, D. A. Dobychkina, Y. S. Yashenkova, D. A. Romanyuk, L. A. Lutova, Local and systemic targets of the MtCLE35–SUNN pathway in the roots of Medicago truncatula. *J. Plant Physiol.* **281**, 153922 (2023).
40. P. Olt, W. Ding, W. X. Schulze, U. Ludewig, The LaCLE35 peptide modifies rootlet density and length in cluster roots of white lupin. *Plant, Cell Environ.* **47**, 1416–1431 (2024).
41. M. Karlo *et al.*, The CLE53–SUNN genetic pathway negatively regulates arbuscular mycorrhiza root colonization in Medicago truncatula. *J. Exp. Bot.* **71**, 4972–4984 (2020).
42. Y. Ma, R. Chen, Nitrogen and phosphorus signaling and transport during legume–rhizobium symbiosis. *Front. Plant Sci.* **12**, 683601 (2021).
43. B. J. Ferguson *et al.*, Legume nodulation: The host controls the party. *Plant Cell Environ.* **42**, 41–51 (2019).
44. K. S. Lay, H. Takahashi, Nutrient-responsive small signaling peptides and their influence on the root system architecture. *Int. J. Mol. Sci.* **19**, 3927 (2018).
45. E. Oh, P. J. Seo, J. Kim, Signaling peptides and receptors coordinating plant root development. *Trends Plant Sci.* **23**, 337–351 (2018).
46. J. Jourquin, H. Fukaki, T. Beeckman, Peptide-receptor signaling controls lateral root development. *Plant Physiol.* **182**, 1645–1656 (2020).
47. T. Araya *et al.*, CLE-CLAVATA1 peptide-receptor signaling module regulates the expansion of plant root systems in a nitrogen-dependent manner. *Proc. Nat. Acad. Sci.* **111**, 2029–2034 (2014).
48. J. Schulze, G. Temple, S. J. Temple, H. Beschow, C. P. Vance, Nitrogen fixation by white lupin under phosphorus deficiency. *Ann. Botany* **98**, 731–740 (2006).
49. A. McKenna *et al.*, The genome analysis toolkit: A MapReduce framework for analyzing next-generation DNA sequencing data. *Genome Res.* **20**, 1297–1303 (2010).
50. P. Cingolani *et al.*, A program for annotating and predicting the effects of single nucleotide polymorphisms, SnpEff: SNPs in the genome of Drosophila melanogaster strain w1118; iso-2; iso-3. *Fly* **6**, 80–92 (2012).
51. A. Abe *et al.*, Genome sequencing reveals agronomically important loci in rice using MutMap. *Nat. Biotechnol.* **30**, 174–178 (2012).
52. J. Jumper *et al.*, Highly accurate protein structure prediction with AlphaFold. *Nature* **596**, 583–589 (2021).
53. M. Mirdita *et al.*, ColabFold: Making protein folding accessible to all. *Nat. Methods* **19**, 679–682 (2022).
54. R. C. Edgar, MUSCLE: Multiple sequence alignment with high accuracy and high throughput. *Nucleic Acids Res.* **32**, 1792–1797 (2004).
55. A. M. Waterhouse, J. B. Procter, D. M. Martin, M. Clamp, G. J. Barton, Jalview version 2–a multiple sequence alignment editor and analysis workbench. *Bioinformatics* **25**, 1189–1191 (2009).
56. F. Lemoine, *et al.*, NGPhylogeny. fr: New generation phylogenetic services for non-specialists. *Nucleic Acids Res.* **47**, W260–W265 (2019).
57. I. Letunic, P. Bork, Interactive Tree of Life (iTOL) v6: Recent updates to the phylogenetic tree display and annotation tool. *Nucleic Acids Res.* **52**, W78–W82 (2024).
58. Y. Pecrix *et al.*, Whole-genome landscape of Medicago truncatula symbiotic genes. *Nature Plants* **4**, 1017–1025 (2018).
59. B. Valliyodan *et al.*, Construction and comparison of three reference-quality genome assemblies for soybean. *Plant J.* **100**, 1066–1082 (2019).
60. S. Sato *et al.*, Genome structure of the legume. Lotus japonicus. *DNA Res.* **15**, 227–239 (2008).
61. B. Hufnagel *et al.*, High-quality genome sequence of white lupin provides insight into soil exploration and seed quality. *Nat. Commun.* **11**, 1–12 (2020).
62. M. J. Sullivan, N. K. Petty, S. A. Beatson, Easyfig: A genome comparison visualizer. *Bioinformatics* **27**, 1009–1010 (2011).
63. B. Lagacherie, M. Bours, J.-J. Giraud, G. Sommer, Interaction entre différentes souches de Rhizobium lupini et les espèces ou cultivars de lupin (Lupinus albus, Lupinus luteus et Lupinus mutabilis). *Agronomie* **3**, 809–816 (1983).
64. M. Martin, Cutadapt removes adapter sequences from high-throughput sequencing reads. *EMBnet. J.* **17**, 10 (2011).
65. D. Tang *et al.*, SRplot: A free online platform for data visualization and graphing. *PLoS One* **18**, e0294236 (2023).
66. L. Marquès *et al.*, Data from "Lupinus albus cluster root temporal RNA-seq." BioProject NCBI. https://www.ncbi.nlm.nih.gov/bioproject/PRJNA1124865. Deposited 13 April 2025.
67. L. Marquès *et al.*, Data from "Lupinus albus cluster root ccr1 mutant RNA-seq." BioProject NCBI. https://www.ncbi.nlm.nih.gov/bioproject/PRJNA1125199. Deposited 13 April 2025.
68. L. Marquès *et al.*, Data from "Lupinus albus whole root phosphate RNA-seq." BioProject NCBI. https://www.ncbi.nlm.nih.gov/bioproject/PRJNA1198000. Deposited 4 May 2025.